Available online at www.sciencedirect.com
ScienceDirect
Trans. Nonferrous Met. Soc. China 35(2025) 2399−2420
Transactions of Nonferrous Metals Society of China
www.tnmsc.cn

Effect of pH-dependent bath speciation on cobalt electrodeposition from sulfate−gluconate solutions

Ewa RUDNIK

Faculty of Non–Ferrous Metals, AGH University of Krakow, Al. Mickiewicza 30, 30-059 Krakow, Poland

Received 21 November 2023; accepted 28 April 2024

Abstract: pH-dependent multiple equilibria in cobalt sulfate−gluconate baths were calculated using stability constants adopted from literature. Changes of the bath speciation were then discussed in terms of spectrophotometric experiments and buffering properties of the solutions (pH 3−10). Cyclic voltammetry indicated changes in electrochemical behavior of cobalt species caused by different ionic compositions of the electrolytes. Tafel slopes were calculated and discussed in relation to electroreduction of cobalt species. Chronoamperometric studies showed 3D instantaneous nucleation of cobalt followed by diffusion-controlled growth, but it was disturbed at higher pH due to the release of cation from gluconate complexes as a limiting step. Diffusion coefficients of cobalt species were found. Changes in the pH were also reflected by modifications of morphology (SEM), development of preferred orientation planes (XRD, texture coefficients) and current efficiency, but not the thickness of the coatings deposited at constant potential of −1.0 V (vs Ag/AgCl). Anodic stripping analysis showed changes in anodic responses originated from the existence of preferentially oriented planes in cobalt layers.

Key words: cobalt; electrodeposition; nucleation; speciation; structure

1 Introduction

Electrodeposited cobalt and its alloys are used widely for various applications ranging from magnetic components and nanowires [1−3] to wear resistant or corrosion protective coatings [4] and composite layers [5,6]. Cobalt coatings characterize with a variety of properties controlled by selection of bath components and pH, temperature, current/potential conditions or external magnetic field [7−13]. Usually, slightly acidic chloride [4,9,10], sulfate [11−13] and chloride−sulfate [5,6,14] solutions are used. Only a small number of studies focusing on the cobalt electrolytes containing complexing agents despite that complex salt solutions are environmentally safe, have improved buffering properties and produce usually adherent bright coatings. The following complexing agents are the most often used: ammonia [15,16], citrate [17,18], gluconate [19,20] and glycine [21,22].

Gluconic acid and its sodium salt are non-corrosive, non-toxic, non-volatile, biodegradable and renewable compounds [23] which can be used as additives in electroplating baths. Both show excellent chelating power to many metal ions and can form stable complexes not only in alkaline and concentrated alkaline solutions, but also in acidic conditions [24]. Gluconate complexing agent can be successfully used for the electrodeposition of heavy metals and alloys [24−28]; nevertheless, the application of this additive in the electroplating of cobalt [19,20] and cobalt alloys [29−34] is rather limited. A literature research in the Scopus data base has shown that there are only two papers considering strictly the electrodeposition of cobalt

Corresponding author: Ewa RUDNIK, E-mail: erudnik@agh.edu.pl
https://doi.org/10.1016/S1003-6326(25)66823-3

from gluconate baths. EL REHIM et al [19] investigated the influence of bath components, pH, current density and temperature on current efficiency, throwing power and microhardness of the coatings. They obtained hard cobalt deposits, which under the optimum conditions were composed of compact microcracked fine grains. The authors also identified instantaneous nucleation model followed by 3D growth under charge transfer control. In turn, RUDNIK and DASHBOLD [20] discussed a role of chloride and sulfate anions in potentiostatic electrodeposition of cobalt from slightly acidic gluconate solutions. It was found that sulfate anions inhibited cathodic process, levelled the coating surface and improved the buffer capacity of the solutions protecting against hydrolysis of cobalt salts at the cathode surface. Progressive nucleation of cobalt followed by 3D growth under diffusion control was identified in the presence of sulfate ions, while this was not strict in the chloride system.

This state of affairs motivated a further analysis of the cobalt electrodeposition from gluconate solutions. The purpose of the present investigations was to determine the influence of pH on speciation and buffering properties of cobalt sulfate−gluconate solutions, kinetics of the electroreduction process, nucleation, morphological and structural properties of the metal layers. This work provides new information on the cobalt electrodeposition from gluconate complexing baths.

2 Experimental

Electrodeposition of cobalt was carried out from solutions containing 0.05 mol/L $CoSO_4$, 0.2 mol/L $C_6H_{11}O_7Na$ and 0.2 mol/L H_3BO_3. The pH of the baths was in a range from 3 to 10 adjusted with H_2SO_4 or NaOH. pH-dependent speciation of the electrolytes was calculated using free available Hyss2009 software. UV−Vis spectra of the solutions were registered (Shimadzu U-2501 PC spectrophotometer) to identify changes in the bath speciation. Buffer capacities of the electrolytes were determined by slow addition (Crison titrator) of 0.1 mol/L HCl or NaOH to a portion of the electrolyte until pH was decreased or increased by unit, respectively. The buffer capacities (β) were calculated according to the following formula [20,26]:

$$\beta = \pm\frac{\Delta n}{\Delta \mathrm{pH}} = \pm\frac{VC}{v\cdot \mathrm{pH}} \quad (1)$$

where Δn is the amount of NaOH or HCl added to the solution necessary to change pH from its initial value by unit (mol); ΔpH is pH change of the solution sample; V is the titrant volume, C is the concentration of titrant (0.1 mol/L), v is the volume of the solution sample (20 cm^3).

Electrochemical measurements were carried out in a three-electrode cell. Glassy carbon as a working electrode (0.196 cm^2) was used due to its non-reactivity with the solution's components and high hydrogen overpotential. A platinum plate (2 cm^2) as a counter electrode and an Ag/AgCl electrode as a reference electrode (all potentials in the further text are referred to this electrode) were used. Non-agitated solution with a volume of 20 cm^3 was used in each electrochemical experiment controlled by potentiostat/galvanostat (Autolab PGSTAT30). Cyclic voltammograms (CV) were registered at a potential scan rate of 10 mV/s. First sweep was always performed from an initial potential of 0.3 V (vs Ag/AgCl) towards more negative values. Chronoamperometric measurements were performed for 40 s at a constant potential from −0.95 to −1.25 V. Anodic stripping analysis (ASA) with a sweep rate of 10 mV/s was performed immediately after potentiostatic metal deposition at fixed potential (40 s) up to 0.5 V without removal of the working electrode from the solution. Potentiostatic cobalt deposition at the potential of −1.0 V was performed for 30 min in the same system using polished copper plates (0.8 cm^2) as universal electrolyte-resistant cathode substrates. All experiments were performed at room temperature.

Morphology of the cobalt layers was examined using scanning electron microscope SEM (Hitachi). The SEM microphotographs were then subjected to image analysis using free available software programs: WxSM4.0beta9.3 for fast Fourier transform (FFT) and Image J for surface profiles. Surface oxygen content was determined by X-ray spectroscopy EDS method (Noran). Crystal structure of the deposits was analyzed by X-ray diffractometry (XRD) (Rikagu diffractometer, Cu K_α radiation).

3 Results and discussion

3.1 Speciation of solutions

Speciation of the sulfate−gluconate solutions was examined by constructing an equilibrium diagram using formation constants summarized in Table 1. Simple metal cation as well as hydroxy, sulfate and gluconate complexes were taken into account over the pH range from 2 to 11. Cobalt−borane species were not considered, since no proper data on the stability constants were reported in accessible literature.

It was assumed that sodium gluconate dissociates completely forming gluconate ions Glu^- (i.e. $C_6H_{11}O_7^-$). The latter can combine with hydrogen ions creating molecules of gluconic acid HGlu in more acidic conditions. Gluconic acid is a polyhydroxylated carboxylic acid of a zig-zag shaped molecule with a labile proton originated from carboxyl group and potentially labile hydroxyl (alcoholic) protons that can be displaced during metal complexation at higher pH. The acid undergoes acid-catalyzed dehydration to form a five- or six-membered cyclic esters (lactones), *γ*-HGlu or *δ*-HGlu, respectively (Fig. 1(a)). The formation of the cyclic structures runs with the reorganization of the acid molecule, and hence it is a much slower process compared to the dissociation of the acid [37]. Both lactones reach an equilibrium very slowly and exist at pH below 4 [36,38], and therefore they were omitted in the equilibrium calculations.

The possibility of deprotonation of alcoholic groups —OH located near the anchor carboxylate group — COOH makes the gluconate ion a powerful chelating agent [21], and thus Glu^- or $H_{-n}Glu^{(n+1)-}$ ligands are formed depending on the pH. Structural formulas of the Co(II)−gluconate complexes are accidentally discussed in the literature [37], although their stoichiometric compositions are known or proposed [37,39,40]. Usually, the structures of complexes represent deductions made by investigators based primarily on the studies of their solutions, so they are not to be regarded as absolutely established [24,37].

Table 1 Equilibrium constants at 298 K [35−37]

Reaction	Equilibrium constant, pK
$Co^{2+}+H_2O \rightleftharpoons CoOH^+ + H^+$	−9.687
$Co^{2+}+2H_2O \rightleftharpoons Co(OH)_2 + 2H^+$	−18.794
$Co^{2+}+3H_2O \rightleftharpoons Co(OH)_3^- + 3H^+$	−31,491
$Co^{2+}+4H_2O \rightleftharpoons Co(OH)_4^{2-} + 4H^+$	−46.288
$2Co^{2+}+H_2O \rightleftharpoons Co_2OH^{3+} + H^+$	−10.997
$Co^{2+}+SO_4^{2-} \rightleftharpoons CoSO_4$	2.36
$Co^{2+}+Glu^- \rightleftharpoons CoGlu^+$	2.31
$Co^{2+}+Glu^- \rightleftharpoons CoH_{-1}Glu + H^+$	−4.96
$Co^{2+}+Glu^- \rightleftharpoons CoH_{-2}Glu^- + 2H^+$	−13.29
$Co^{2+}+3Glu^- \rightleftharpoons CoH_{-1}Glu_3^{2-} + H^+$	−1.27
$Co^{2+}+3Glu^- \rightleftharpoons CoH_{-2}Glu_3^{3-} + 2H^+$	−9.21
$2Co^{2+}+2Glu^- \rightleftharpoons Co_2H_{-3}Glu_2^- + 3H^+$	−17.89
$H^+ + SO_4^{2-} \rightleftharpoons HSO_4^-$	1.12
$H^+ + Glu^- \rightleftharpoons HGlu$	3.35
$HGlu \rightleftharpoons \gamma\text{-}HGlu + H_2O$	−0.68
$HGlu \rightleftharpoons \delta\text{-}HGlu + H_2O$	−1.15

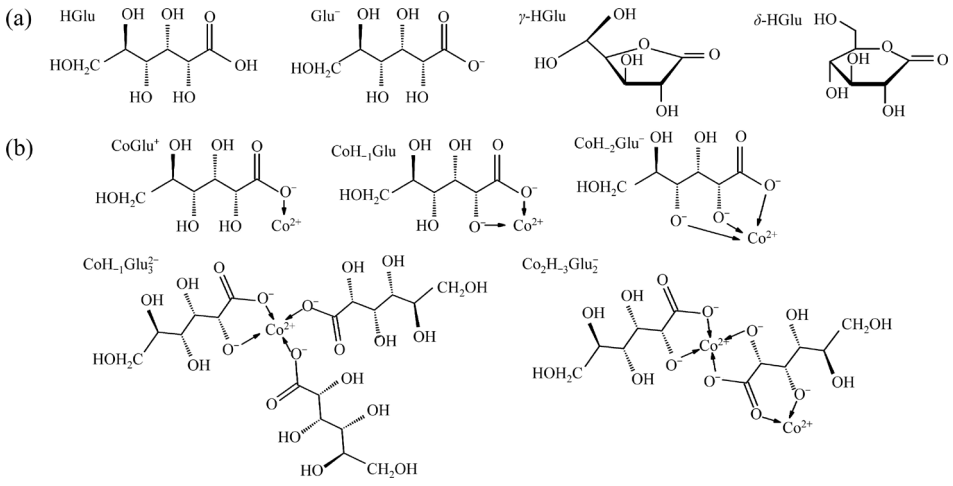

Fig. 1 Simplified structures of gluconic acid species (a) and cobalt(II)−gluconate complexes (b)

Figure 1(b) shows exemplary simplified structures of the cobalt−gluconate species that can exist in the electrolyte. It should be emphasized that structures of the chelates can involve water molecules to maintain octahedral coordination of the Co(II) cation [37].

Literature data on the cobalt−gluconate complexes are scarce. ASHTON and PICKERING [37] reported the presence of an unstable cationic species of $Co(C_6H_{11}O_7)^+$ (i.e. $CoGlu^+$ in this study) in solutions of pH below 7.5. An anionic species (not specified), which can subject to rapid auto-oxidation was postulated above pH 9.5, while in the intermediate pH range two insoluble cobalt−gluconate compounds, $Co_2(OH)_3Glu\cdot H_2O$ and $Co_3(OH)_2Glu_2\cdot 2H_2O$, were identified. ESCANDAR et al [39] confirmed the existence of the complex with 1:1 stoichiometry, but they did not observe precipitation of insoluble species with increasing cobalt to ligand concentration ratios. The authors stated that in such conditions, coordination of the metal ion by the secondary alcohol (hydroxyl) groups became important due to displacing of protons, and therefore soluble anionic complexes with chelate rings (e.g. $CoH_{-1}Glu_3^{2-}$, $CoH_{-2}Glu_3^{3-}$, $Co_2H_{-3}Glu_2^-$) were recommended. NMR spectra registered at pH of 10 in an excess of gluconate acid confirmed that the metal ion is octahedrally bonded to carboxyl of C^1 carbon atom and alcoholic group of C^2 atom of three ligand molecules. The authors supposed that —OH group at C^3 atom can participate in chelation of the cobalt cation by hydrogen bonding between this hydroxyl proton and the oxygen electron lone pairs of either the carboxylate group or the hydroxyl of C^2 carbon atom. Other studies [40] specified the existence of $CoGlu^+$ at pH below 7.3, $CoGlu(OH)_2$ for pH above 11.8 and $Co_2Glu_2(OH)$ in the intermediate pH range.

For the baths used in this study, main cobaltous components at acidic conditions (2<pH< 5) are Co^{2+} (as aqua complex), $CoSO_4$ and $CoGlu^+$ (Fig. 2). At higher pH, neutral or various anionic chelate complexes can exist. They are composed of Co(II) cation and one or three gluconate species deficient with hydrogen ions originated from carboxyl group —COOH (indicated here as Glu^-) and hydroxyl groups —OH (indicated here as H_{-n}). The highest cobalt fractions of the dominant complexes are 53% $CoSO_4$ at pH 2.0, 70% $CoGlu^-$ at pH 4.0, 76% $CoH_{-1}Glu_3^{2-}$ at pH 6.7 and 96% $CoH_{-2}Glu_3^{3-}$ at pH 10.0. Theoretical calculations predicted also the presence of dimeric form $Co_2H_{-3}Glu_2^-$ with their maximal concentrations of 1×10^{-6} mol/L at pH of about 8. Soluble hydroxy-complexes remained in negligible concentrations, i.e. below 10^{-7} mol/L, in the entire pH range. Thus, they are not shown in Fig. 2.

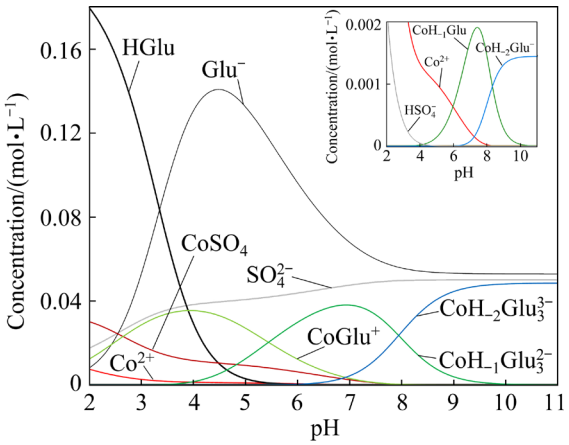

Fig. 2 pH-dependent speciation of cobalt sulfate−gluconate baths

The cobalt solutions were further investigated by UV−Vis spectrophotometry to identify changes in their speciation (Fig. 3). For comparison, cobalt sulfate solution free of additives of pH 3 was also used. The absorption spectrum for pure cobalt sulfate solution (inset in Fig. 3(a)) corresponds to d−d transitions in octahedral aqua complex $[Co(H_2O)_6]^{2+}$: $^4T_{1g}(P)\leftarrow{}^4T_{1g}(F)$ associated with the absorption band at the wavelength of 510 nm and 2 electron $^4A_{2g}\leftarrow{}^4T_{1g}(F)$ revealed as a broad absorption peak of low intensity at the wavelength of about 650 nm [32,37]. The first band showed a shoulder in a higher energy region at about 470 nm. It appears from the short wavelengths of the absorption spectrum in view of the fact that the spin orbit interaction in the excited state $^4T_{1g}(P)$ removes the degeneracy [41,42].

Addition of sodium gluconate to the cobalt sulfate solution at the same pH changed slightly the absorption spectra with a shift of the maximum wavelength of the first peak by a few nanometers (Fig. 4). It should be emphasized that in aqueous solutions, free Co^{2+} ions or those bonded in the complexes are hydrated by water molecules to satisfy octahedral geometry (e.g. $[CoGlu(H_2O)_3]^+$) affecting the shape of the absorption spectra [39]. A

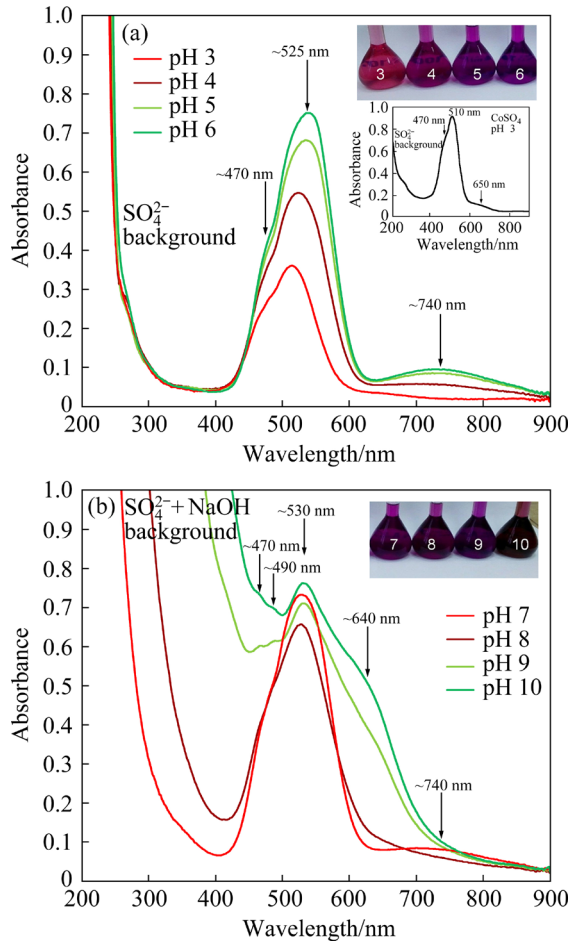

Fig. 3 UV−Vis spectra of cobalt sulfate−gluconate solutions of different pH: (a) 3−6 (Inset: spectrum of $CoSO_4$ solution, pH 3); (b) 7−10

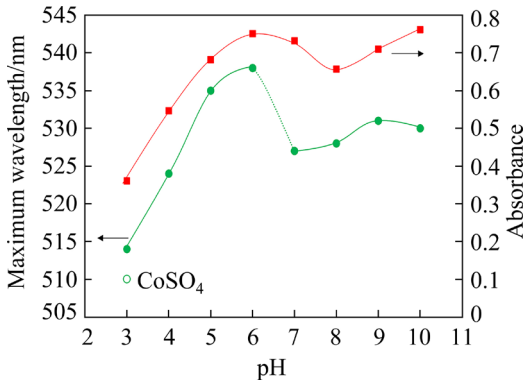

Fig. 4 Influence of pH on absorbance and maximum wavelength of main absorption band of cobalt solutions

shift in the position of the absorption spectrum in the visible range indicates that the cobalt ions in the gluconate solution are in a stronger ligand field environment [37].

The most evident differences in the absorption spectra of the gluconate solutions were observed for four pH ranges: 3−4, 5−6, 7−8 and 9−10. For pH values from 3 to 6, the main peak at about 525 nm got higher with simultaneous shifting its maximum from 514 to 538 nm. Then, the absorption band became reduced for pH 7 and 8 with sudden decrease in the maximum wavelength to 527 nm. This was followed by renewed growth of the absorption for higher pH values at somewhat longer light wavelengths of 530−531 nm. The main maximum was preceded by small shoulder at about 470 nm, which turned into two weak signals at 460 and 490 nm for pH values of 9 and 10. Low wide absorption band was also observed at 740 nm. Its maximum increased with pH from 4 to 6, while it disappeared for the most acidic (pH 3) and more alkaline solutions (pH 8 or higher). At pH values of 9 and 10, one new weak shoulder appeared at about 640 nm. The absorbance registered in the UV region (below 400 nm) is attributed to other transitions in the solution background components such as sulfate ions and sodium hydroxide. The modifications in the absorption spectra are correlated with changes in the solution's color from pink to violet for pH from 3 to 5, and further from violet-purple to final wine-red for pH 9−10.

The changes in the solution's spectra originate from their ionic speciation. At lower pH values, the carboxyl groups of gluconic acid may be partially protonated affecting their ability to form complexes with cobalt(II) ions. As pH increases, protonation decreases, which in turn enhances the ability of gluconic acid to form more stable complexes with cobalt(II) ions due to an increase in the number of possible coordination bonds with the ligand (Fig. 1). The calculations of ionic equilibria (Fig. 2) clearly indicate that modification of the solution pH affects the composition and structure (geometry) of the Co(II)−gluconate complexes. Such structural changes determine the ligand field effect: the energy of the d orbitals in the metal ions and the electron transitions in the complexes. The energy absorbed by the electron to d−d transitions corresponds to the crystal field splitting. Consequently, the lower the splitting energy difference (ΔE), the lower energy light waves (i.e. higher wavelength, λ) would be absorbed according to the following relationship [41]:

$$\Delta E = h\nu = \frac{hc}{\lambda} \tag{2}$$

where h is Planck constant, ν is the wave frequency, and c is the speed of light in vacuum. This

consequently leads to shifting of the wavelength at which the light absorption is the most pronounced in the UV−Vis spectra (Fig. 4).

Total light absorption by the gluconate solutions is dependent on both molar concentration of the individual species (c_i) and their molar absorptivity (ε_i). Therefore, when the Beer−Lambert law is obeyed at given wavelength (λ_i) for the particular component i, the absorption A_λ of a mixture of the complexes is given by the following formula [41]:

$$A_{\lambda_i} = \sum_i (\varepsilon_{i,\lambda_i} \cdot c_i \cdot l) \tag{3}$$

where l is a path length.

Equation (3) shows that the development of the absorption signals cannot be unambiguously attributed in this study to the particular cobalt species due to rather complicated speciation of the solutions and different wavelengths of the light absorbed by particular molecules or ions. Nevertheless, it can be accepted that combination of Co^{2+} and $CoSO_4$ gives three characteristic bands at 470, 510 and 650 nm. The presence of $CoGlu^+$ does not change the shape of the spectrum but shifts the maximum wavelengths towards higher values. A much greater influence on the spectrum displays the pH-dependent change in the composition of the ligand resulted from the complexation of the cobalt ions also by deprotonated alcohol groups. This is indicated by sudden reducing of the maximum wavelength at pH 7−8 where $CoH_{-1}Glu_3^{2-}$ and $CoH_{-1}Glu$ show their highest fractions. Moreover, the absorption band at 740 nm can be attributed to the presence of both species as it develops in the pH range of 4−7 where their predicted concentrations raise in the baths. Finally, all bands including small shoulders at 490 and 640 nm observed for the most alkaline solutions can confirm the presence of anionic complexes of more complicated structures like $CoH_{-2}Glu_3^{3-}$ and $CoH_{-2}Glu^-$. Such different forms are in the equilibrium in the solution (Fig. 2) and exhibit peculiar absorption peaks. On the other hand, the complexes can exist also in different geometric conformations having slightly different light absorption properties indicated by shoulders at the absorption peak.

The spectrophotometric studies of the cobalt−gluconate solutions were reported previously by ASHTON and PICKERING [37]. They discussed a growth of the main peak at 520 nm for various Co(II):gluconate ratios and the peak was ascribed to the formation of the $CoGlu^+$ species (pure sodium gluconate solution gave the absorbance signal at about 420 nm). Addition of sodium hydroxide to the solutions containing equal amounts of cobalt nitrate and sodium gluconate caused slight color changes where spectral transmittance curves indicated the formation of a second absorption peak at 495 nm and, in the presence of excess alkali, a decrease in the intensity of the 520 nm peak. The latter was illustrated for 510 nm and approximate pH of 7.5−8.8. There was also some general broadening in the alkaline solutions attributed to autooxidation, but no specified compounds were shown. The precipitation of gelous compound $Co_2(OH)_2Glu\cdot xH_2O$ was observed after a few days in the solutions having pH between 7.5 and 9.5. It is worth to note that in the current study, all cobalt−gluconate solutions are stable even after two years after preparation. ESCANDAR et al [39] confirmed a shift of the band from 509 to 521 nm with increasing pH from 2.7 to 8.6. More recently, WESTON et al [32] showed changes in the absorption spectra for $CoSO_4$/gluconate ratios of 1:2 and 1:10 at pH 6.0, but they did not discuss them in details.

3.2 Buffering properties

It is known that solution resistance to pH changing during electrolysis is an essential factor for deposition of pure metal. Coevolution of hydrogen at a cathode surface is often accompanied by fast alkalization of the electrolyte adjacent to the electrode (up to 5 units in 30 s) [43] causing precipitation of hydroxides and basic salts [13], which are then built up into the growing metal layer producing porous metallic structure [44]. Hydrogen atoms formed during electroreduction of protons can also penetrate the metallic lattice due to their smallest dimensions among all elements. This affects the metal structure [45] and gives marked mechanical effects, such as hydrogen embrittlement [46]. Both phenomena lead to worsening properties of the metallic layer, and hence the electrolytes of high buffer capacities should be used to protect against the unfavorable effects.

In this study, two bath components were intentionally added to the cobalt solutions as the buffering agents, i.e. boric acid and sodium gluconate. Analysis of the bath speciation (Fig. 2)

appears that the SO_4^{2-}/HSO_4^- pair and the cobalt complexes can also participate under the buffering effect by setting up pH-dependent equilibria. Figure 5 shows buffer capacities of the solutions used in this work. They were determined as the quantity of strong acid HCl or base NaOH needed to change the pH of 1 L solution by one pH unit.

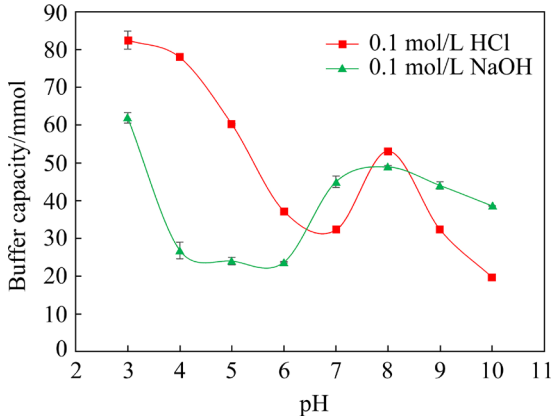

Fig. 5 pH-dependent buffer capacities of cobalt sulfate−gluconate solutions for acid or base addition

It was found that the solutions of acidic pH showed higher buffer capacities for acid than for base addition, although they decreased in both cases with increased bath alkalization. The buffer capacities improved unexpectedly for pH 8, but it was followed by further worsening.

For all electrolytes, buffering effect can also arouse from the presence of weak boric acid. It can dissociate in aqueous solution in three steps by detaching successive hydrogen ions [47]. The distribution of boric species depends on the dissociation constants, which have relatively low values. Therefore, boric acid exists in a molecular form in acid and neutral environments giving equimolar molecular/ionic ratio at about pH 9 (Fig. 6(a)). At the concentrations higher than 0.01 mol/L, H_3BO_3 acts as a Lewis acid by accepting hydroxyl ions to form hydroxyborate ions $B(OH)_4^-$ and polyborates [48,49]. Thus in the pH range from about 7 to 10, triborate species appears as a third main component in the boric acid speciation with their highest fractions at pH of 8−10 (Fig. 6(b)). The boric acid speciation shows that their main buffering activity is in the alkaline media, and hence this behavior can be responsible for the increasing buffering properties during NaOH addition observed in the cobalt−gluconate solutions of pH 7−10 (Fig. 5).

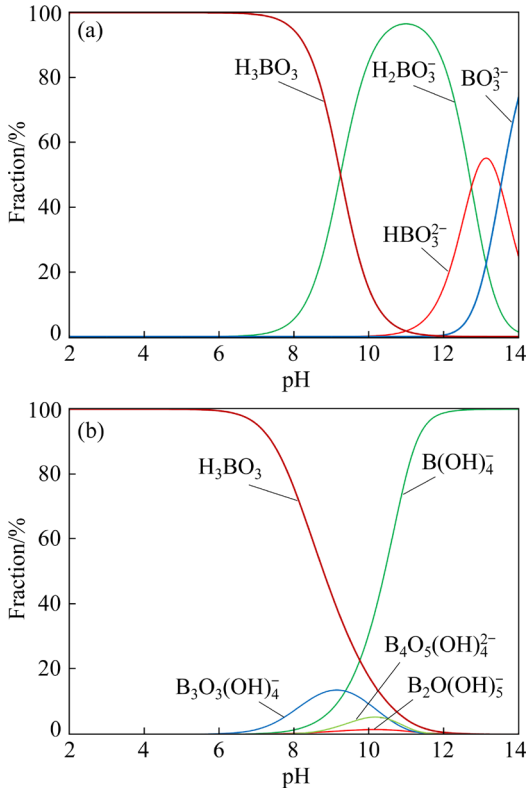

Fig. 6 Equilibrium distribution of species in 0.2 mol/L H_3BO_3 dissociated into borates (a) or polyborates (b) (Equilibrium constants are taken from Refs. [47,49])

The gluconate and sulfate species can also neutralize excessive H^+ and OH^- ions by establishing the following equilibria:

$$HGlu \rightleftharpoons^{H^+} Glu^- + H^+ \rightleftharpoons^{OH^-} Glu^- + H_2O \quad (4)$$

$$HSO_4^- \rightleftharpoons^{H^+} SO_4^{2-} + H^+ \rightleftharpoons^{OH^-} SO_4^{2-} + H_2O \quad (5)$$

The presence of gluconate species is very favorable in terms of buffering action of the acidic solutions. At pH about 3.4 there are equimolar amounts of undissociated and dissociated forms (Fig. 2), and hence the buffer capacity of this weak acid reaches its maximum value for pH=pK_a=3.35 (Table 1). For pH values higher than pK_a, the buffer capacity of the HGlu−Glu^- system decreases. In turn, the sulfate pair (Eq. (5)) seems not to play a principal role in the buffering action, since HSO_4^- concentrations are low and they rapidly decrease in a pH range of 2−4 (inset in Fig. 2). Equilibria (4) and (5) are in a good agreement with the changes of the buffer capacity of the acidic cobaltous electrolytes and well explain their higher protective properties for the acid addition, which originate mainly from high fraction of the Glu^- species (Fig. 2) that can easy recombine with added H^+ ions.

In turn, the values of the buffer capacities towards strong base addition stabilize at low but constant level at pH of 4−6. This is understandable since Glu^- and SO_4^{2-} ions have no possibility to combine with OH^-. However, the latter can indirectly affect the equilibria of cobalt complexation via changes in the Glu^- concentration.

Improved buffering at pH 8 for the acid addition is definitely related to the equilibria involving equimolar amounts of anionic cobalt complexes $CoH_{-2}Glu_3^{3-}$ and $CoH_{-1}Glu_3^{2-}$ due to pH-dependent equilibrium between both species:

$$CoH_{-1}Glu_3^{2-} \rightleftharpoons CoH_{-2}Glu_3^{3-} + H^+ \quad (6)$$

For more alkaline conditions, neutralization of excessive amounts of strong acid is less effective via transformation of cobaltous complexes, since it is affected solely by the balance between dominant $CoH_{-2}Glu_3^{3-}$ and $CoH_{-2}Glu^-$ of low concentration. It may be also accepted that equilibrium (6) is not important in the bath protection against pH change caused by the base addition at pH above 9, since the concentrations of both complexes are practically stable (Fig. 2).

The above discussion shows that protection of the electrolyte against pH change is a consequence of multiple ionic equilibria occurring in the baths. It involves not only typical buffering agents but also formation of the metal complexes. Therefore, it may be expected that at longer electrolysis time the speciation of the electrolyte adjacent to the cathode may fluctuate affecting electroreduction processes. SANTOS et al [13] showed that the buffer contribution of this acid was effective in the cobalt electrodeposition from sulfate bath (pH=5.0) only at room temperature, while cobalt hydroxide precipitated simultaneously with cobalt deposition as the electrolyte was heated. In turn, enhanced buffering behavior of the gluconate system was confirmed in other studies indicating much better properties if combined with sulfate than chloride ions present in the acidic solution [20,28,50].

3.3 Voltammetric studies

The cyclic voltammetric measurements were realized on a glassy carbon electrode due to high hydrogen overpotential (about 0.5 V) on such substrate [51]. Figure 7 shows that electrodeposition

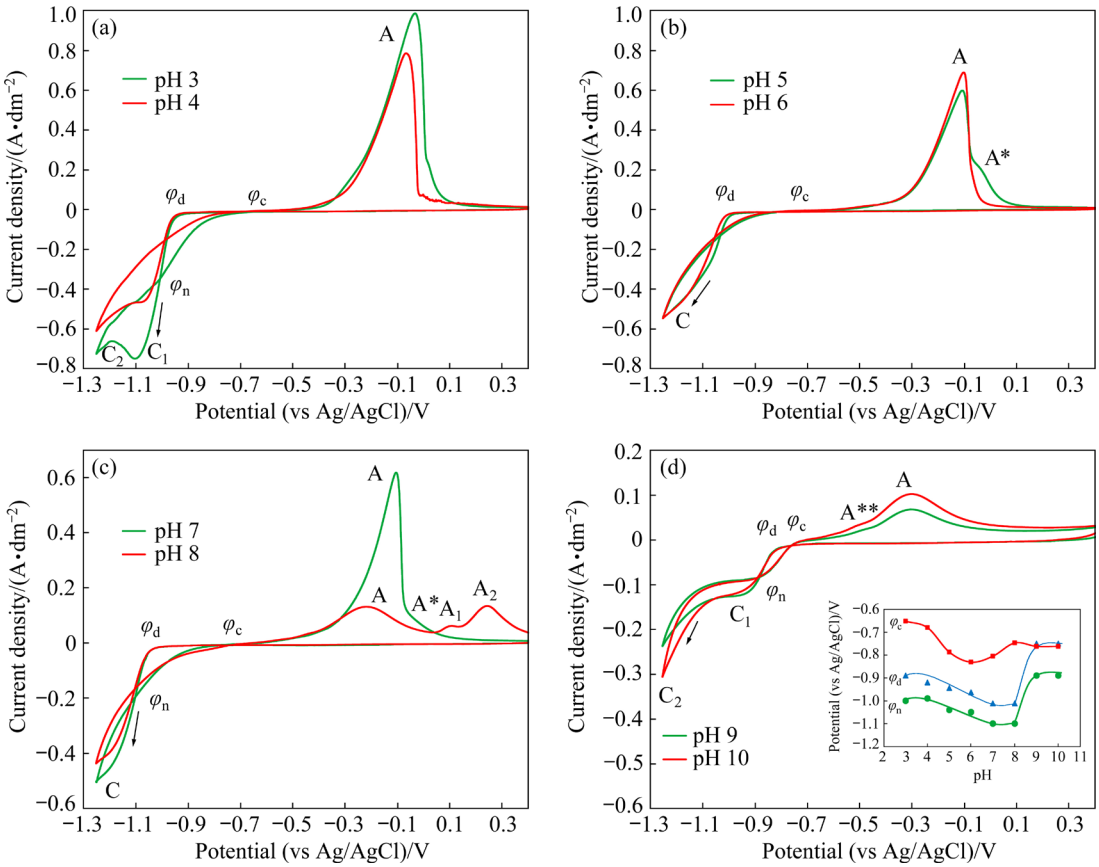

Fig. 7 Cyclic voltammetric curves for cobalt gluconate solutions of various pH (Inset: influence of pH on deposition (φ_d), nucleation (φ_n) and crossover (φ_c) potentials)

of cobalt begins at potentials dependent on the pH. Cathodic process started below −0.92 V at pH 3, but then the potential moved a little towards more negative values up to −1.03 V while pH increased to 8. In the most alkaline baths, behavior of the system changed and reduction was observed even at more positive potential (−0.81 V). Simultaneously, the shape of the curves was modified. For pH 3 and 4, a clear cathodic peak C_1 corresponding to the reduction of cobalt ions was formed at the potential of about −1.1 V. Its height gradually disappeared with alkalization resulting finally in a plateau on cathodic branches for pH 9 and 10. In all cases, the cathodic branches involve two electroreduction processes, since cobalt deposition is practically indistinguishable from hydrogen evolution reaction as represented by slightly separated signal C_2 (pH 3−4 and 9−10) or overlapped currents C (pH 5−8).

During the reverse scan, two characteristic crossovers between the branches for the negative and positive sweeps were observed. At more negative potentials loops typical for the nucleation and growth of a new phase were found. Nucleation potentials (φ_n) (i.e. crossover potential at the nucleation loop) associated with electrocatalytic points [51] were shifted with pH (inset in Fig. 5) in the range from −0.89 to −1.10 V. These values are usually affected by the bath composition and for example, in citrate solution (pH 4.8) nucleation potential was −0.93 V (vs Ag/AgCl) [17], while for the ammoniacal system (pH 4.7) it was −1.1 V [52]. Second crossover potentials (φ_c) are generally related to thermodynamic potential of M/M^{z+} electrodes. These appeared at approximately −0.7 V and were more negative than equilibrium potential for simple Co/Co^{2+} electrode (−0.54 V vs Ag/AgCl) due to the presence of cobalt complex species instead of free cations. The cathodic currents recorded between the nucleation potential (φ_n) and second crossover potential (φ_c) were higher during the reverse sweep than during the forward sweep for each bath. It is obvious, since energy required for cobalt overpotential deposition on foreign substrate is higher than that for the metal deposition on the native layer formed during the previous scan [51].

The positive scan revealed anodic peaks A of the cobalt electrochemical dissolution. The height of the anodic signals decreased with increased pH corresponding to gradual inhibition of the preceding cathodic process. Simultaneously, shape and amount of the anodic peaks change indicating additional reactions at the electrode surface like subsequent formation of gluconate complexes of $CoGlu^+$ or $CoH_{-n}Glu_3^{-(n+1)}$. In the most alkaline solutions the main anodic peak is preceded by a small bend at about −0.5 V, which can be attributed to cobalt hydroxide intermediate [13]. It can hinder the dissolution of the metallic phase and, thus, further formation of the soluble complexes giving finally wide anodic peak (Fig. 7(d)). Cobalt oxides do not appear to be produced during anodic scanning because their precipitation does not proceed to any appreciable rate until potentials of about 0.3−0.4 V are reached in a very alkaline gluconate bath (0.5 mol/L NaOH) [53].

Analysis of the cathodic branches of voltammetric curves shows that deposition of cobalt is governed by the form of the electroactive species and release of the cation from individual complexes can be considered as rate-determining step, especially in more alkaline conditions where limiting currents were observed. This may be confirmed by anodic peaks developed during reverse scans. They were getting smaller and shifted towards more negative potentials with increased pH showing continuing inhibition of the metal electrodeposition.

Figure 8 shows the voltammetric cathodic curves plotted in the $\varphi-\lg J$ coordination system. It was simplified that a potential of the electrode is proportional to cathodic overpotential, and thus linear ranges of the curves were described by the following equation [51]:

$$\varphi=a+b\lg J=\frac{2.303RT}{\alpha_C zF}\lg J_0-\frac{2.303RT}{\alpha_C zF}\lg J \quad (7)$$

where J_0 is the exchange current density, α_C is the cathodic transfer coefficient, R is the molar gaseous constant, T is the thermodynamic temperature, F is the Faraday constant, and z is the number of electrons involved in the activation step in a multistep cobalt deposition.

Linear parts of the curves correspond to the current/potential range of charge transfer as a rate-determining step of cobalt electrodeposition. It was found that the "Tafel slopes" change within three pH ranges of 3−4, 5−8 and 9−10 giving values of (0.063±0.000) V/dec, (0.075±0.004) V/dec and (0.123±0.004) V/dec, respectively. The plots shown

in Fig. 8 can be used directly to measure the transfer coefficients α_C according to Eq. (7), where $-2.303RT/(\alpha_C zF)$ corresponds to the slopes.

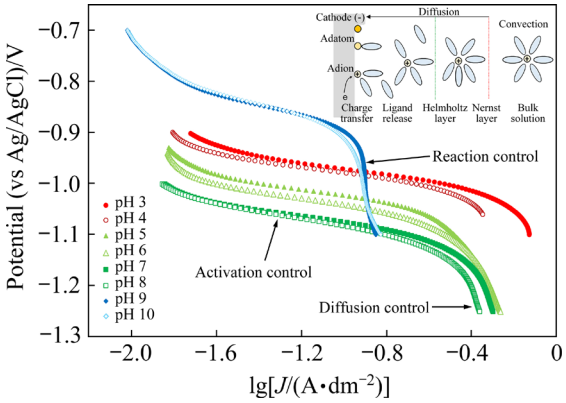

Fig. 8 Cathodic polarization curves plotted in $\varphi-\lg J$ coordination system (Inset: consecutive electroreduction stages for complex metal cation)

It is worth to emphasize that definition of transfer coefficient applies only to an electrode reaction that consists of a single elementary step involving the simultaneous uptake of z electrons from the electrode in the case of α_C [54]. However, the elementary step of cathodic reaction involving the simultaneous uptake of more than one electron is regarded to be highly improbable and the majority of electrode reactions do not consist of a single elementary step, but rather, they are multistep, multi-electron processes. Therefore, the mechanistic interpretation of an electrode process becomes quite complicated if the formal potentials of two consecutive one-electron transfer steps are very close or the process includes adsorption of intermediates and combination or dissociation rate-determining steps. Table 2 summarizes the results of the calculations based on the values of the Tafel slopes. Denoting the resulting "cathodic quantity" by $\alpha_C z$, the general values of α_C for z=2 and z for assumed α_C=0.5 were found. The resulting z value is then identified with the number of the electrons involved in a hypothetical rate-determining step or with that involved in the overall electrode reaction. Independently on the interpretation way used, it is clearly visible that in three ranges of pH various electroactive cobalt species participate in the rate-determining step (i.e. charge transfer) of the cathodic reaction. For pH 3−4, α_C is close to theoretical value of 0.5 indicating reduction of Co^{2+} originated from labile

Table 2 Parameters for cobalt deposition upon data shown in Fig. 8

Solution pH	Tafel slope, b/(V·dec^{-1})	Transfer coefficient for z=2, α_C	Number of electrons for α_C=0.5, z
3	0.063	0.47	1.9
4	0.063	0.47	1.9
5	0.072	0.41	1.6
6	0.078	0.38	1.5
7	0.072	0.41	1.6
8	0.080	0.37	1.5
9	0.119	0.25	1.0
10	0.125	0.24	0.9

$CoGlu^+$ complex. Thus, a former step of the release of metal cation from the complex seems to be very fast, while cathodic reduction involves two steps of single electron transfer. In the pH range of 5−8, speciation of the bath gives $CoH_{-1}Glu_3^{2-}$ as dominating form representing chelate complex composed of three gluconate species, while electrochemistry of the process complicates and multistep reduction including a sequence of events can take place. Each step should have "own" kinetic parameters, but the experimental curve is similar to be previously with only higher slope value. It may be assumed that each step of electron transfer run in the same potential range, but general α_C value can involve number of electrons transferred in quasi-equilibrium prior to the rate-determining step (e.g. non-rate limiting reduction of intermediate species) and contribution from rate-determining step, i.e. $\alpha_C=\gamma+\alpha_{C,rds}z_{rds}$ [55]. This can give the fractional value of electrons calculated for total α_C of 0.5. $CoH_{-1}Glu_3^{2-}$ is chelate complex, and thus it cannot be considered as an electroactive species. It is believed that in the neighborhood of the cathode gluconate ligands are gradually released from anionic species giving more simple structure in intermediate species undergoing one-electron reduction at the cathode surface, e.g. $CoOH^+$. It is then followed by reduction of cobalt ion to metallic form [9]. Finally, in the most alkaline conditions the Tafel slopes were of 0.12 V/dec, while the reaction includes one electron in the rate-determining step. This may suggest that coverage of the cathode by intermediates increases seriously and potential-dependent rates can still arise due to an electrochemical desorption. It is combined with a release

of electroactive species from the chelate complex giving chemical reaction as a rate- determining step visible in the CV curves as limiting currents for pH 9 and 10.

3.4 Initial stages of electrodeposition

The influence of pH on initial stages of the cobalt electrodeposition was investigated. Figure 9 shows chronoamperometric curves registered at constant cathode potentials. Two types of the transients were observed. For pH 3−7, the curves show a gradual increase in the cathodic current up to a maximum for all potentials (at shorter time for more negative potentials) with their final part falling to the plateau. The shape of the J−t curves is typical for three-dimensional nucleation and growth process occurring under the mass transfer control. In turn, for more alkaline baths (pH 8−10), after charging the double layer, cathodic currents decrease immediately to plateau and no nucleation peaks are developed. This can be related to a release of the cation from complex structure as a the slowest step of the electroreduction.

The rise of the current in the J−t plots for pH 3−7 corresponds to the increase of the electroactive area due to the growth of the individual isolated metal nuclei and/or the increase of the number of nuclei. At this step transport of the electroactive species to the growing centers occurs through hemispherical diffusion zones formed around each isolated nucleus. Radii of the hemispherical zones increase with time and the diffusion zones start to overlap forming finally a planar diffusion layer. The maximum of the cathodic current at short time is related to the maximal electroactive area, i.e. the moment at which hemispherical metal nuclei are on the point of the collision.

The falling part of the curves are characterized by the Cottrell equation, since the electrochemical reduction run under linear diffusion [51]:

$$J=-\frac{zFD^{1/2}C}{\pi^{1/2}t^{1/2}} \tag{8}$$

where D is the diffusion coefficient of cobalt ions, C is the concentration of metal ions, and t is the time.

Figure 10 shows analysis of the falling part of J−t curves according to Eq. (8) for exemplary deposition potential of −1.2 V. Linear parts of the J−$t^{-1/2}$ curves were observed for all baths, although only for pH 3 straight line intersects the origin of the coordination system. Diffusion coefficients for cobalt ions were estimated. The values of 1.6×10^{-5} cm^2/s for pH 3 and 2.6×10^{-6} cm^2/s for pH 4 are similar to typical diffusion coefficients reported for cobalt ions in cobalt sulfate containing aqueous solutions, i.e. 10^{-6}−10^{-5} cm^2/s [55,56]. In turn, for pH 5 and higher the diffusion coefficients were lower, i.e. $(6.2\pm2.2)\times10^{-7}$ cm^2/s. This is correlated with the speciations of the baths (Fig. 2) showing inhibition of the mass transport due to formation of cobalt complexes with more advanced structure. It is worth noting that in complex system all particles containing metal cation participate in the mass transport, but only a part of them can be electroactive species [57]. This may cause the J−$t^{-1/2}$ relationship to deviate from ideal linearity, especially with regard to the existence of other steps in electrochemical reactions, such as the formation of intermediates, surface diffusion of electroactive species, and the release of metal ion from chelate complexes.

Potentiostatic current transients for metal nucleation and theoretical background for different nucleation modes were discussed by various authors. The most often, instantaneous and progressive nucleation of three dimensional hemispherical nuclei is considered according to the models proposed by SHARIFKER and HILLS [58], where classification of the nucleation type is based on a comparison of the experimental results with theoretical curves. During instantaneous nucleation all nuclei are generated simultaneously and they grow further with the same rate. Under such conditions the following diagnostic equation is satisfied:

$$\left(\frac{J}{J_{\max}}\right)^2=\frac{1.9542}{t/t_{\max}}\left[1-\exp\left(-1.2564\frac{t}{t_{\max}}\right)\right]^2 \tag{9}$$

During progressive nucleation the nuclei are formed constantly and they grow to different sizes and/or at different rates. In this case suitable expression is

$$\left(\frac{J}{J_{\max}}\right)^2=\frac{1.2254}{t/t_{\max}}\left[1-\exp\left(-2.3367\left(\frac{t}{t_{\max}}\right)^2\right)\right]^2 \tag{10}$$

Figure 11 shows exemplary non-dimensional plots of the nucleation models and the experimental

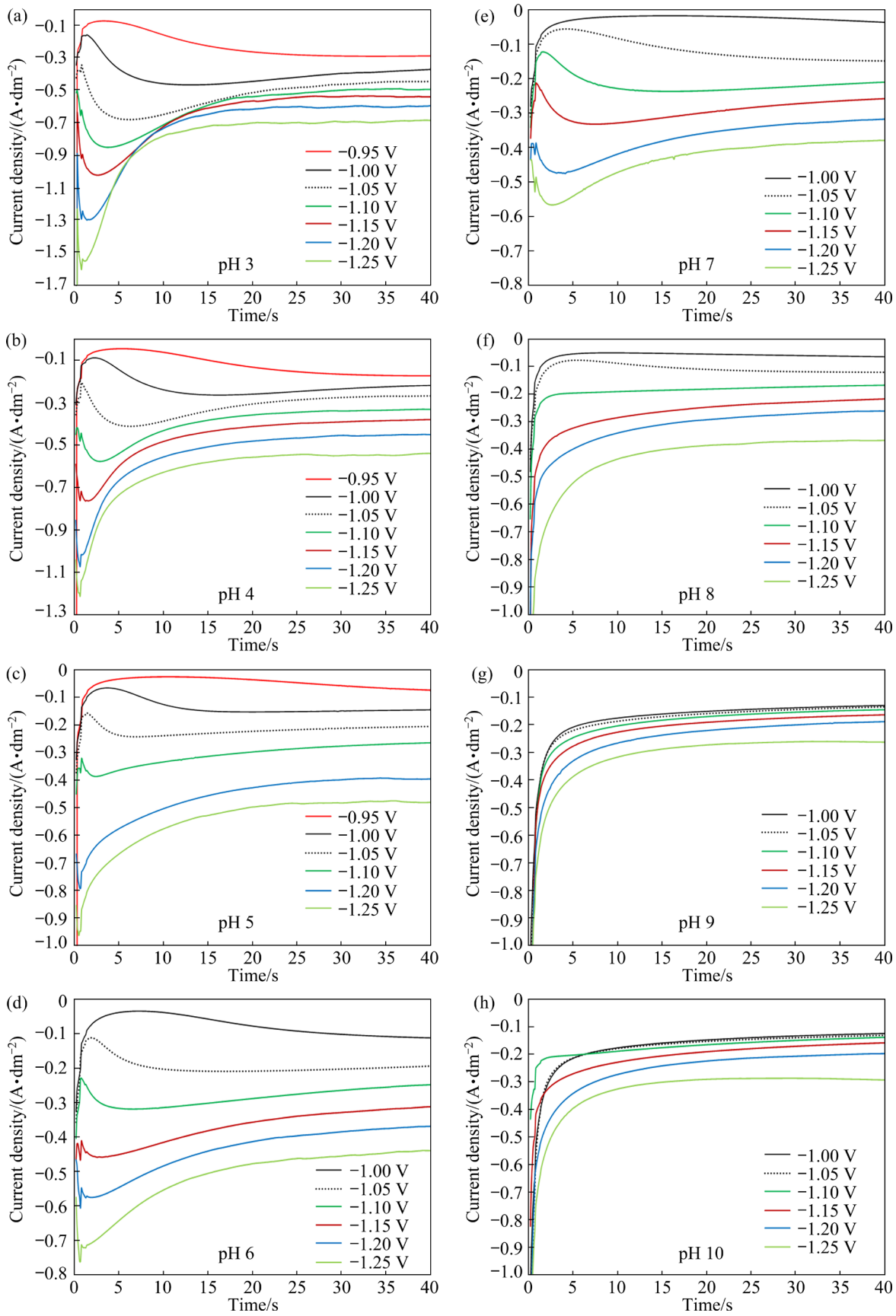

Fig. 9 Chronoamperometric curves for cobalt deposition registered at various potentials and solution pH: (a) pH 3; (b) pH 4; (c) pH 5; (d) pH 6; (e) pH 7; (f) pH 8; (g) pH 9; (h) pH 10

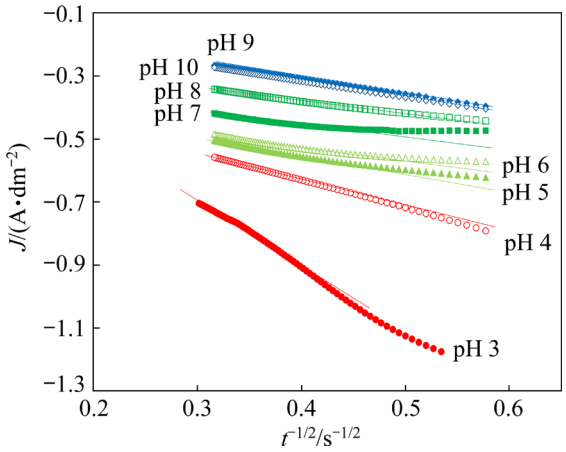

Fig. 10 Analysis of falling part of J−t curves according to Cottrell equation

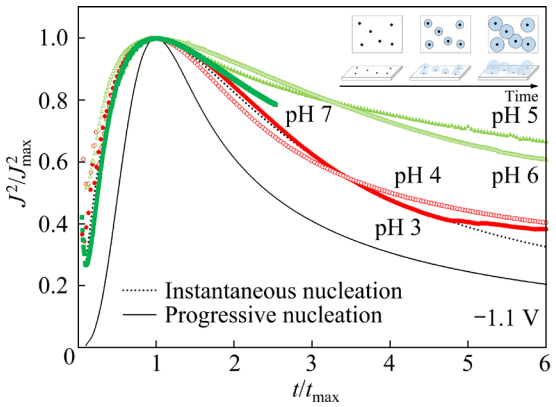

Fig. 11 Interpretation of J−t transients according to nucleation models developed by SHARIFKER and HILLS [59] for deposition potential of −1.1 V and graphical representation of nuclei growth during instantaneous nucleation model

chronoamperometric data for pH 3−7, where characteristic apparent maxima on the J−t curves were developed (for potentials more positive than −1.1 V, the cathodic peaks were less noticeable on the J−t curves, and thus their unambiguous analysis was not possible). Very good agreement of the experimental and theoretical predictions for instantaneous nucleation was observed (also for other deposition potentials not shown), although at longer deposition stages deviations from the predicted curve appeared. The latter was more emphasized with increased solution pH. This is well correlated with changes of the bath speciation and all observations discussed above, since more harder release of metal cations from complexes hinders deposition of the metal. It is also noteworthy that the SHARIFKER and HILLS model is valid primarily for fast electrochemical processes with high exchange current densities [58]. Electrodeposition of cobalt is not one of these cases, and moreover, it is accompanied by hydrogen coevolution due to the relatively low hydrogen overvoltage. However, the ranges of well overlapping experimental and theoretical curves indicate that hydrogen coevolution does not seriously disrupt the first stage of metal formation. This concurrent process can affect the values of the measured cathodic currents when larger cobalt nuclei are formed, since at the very initial period of the deposition the hydrogen evolution is inhibited due to the use of glassy carbon as a substrate of high hydrogen evolution overvoltage [51].

For accepted diffusion-controlled instantaneous model of the metal electro-crystallization the following set of equations can be used for calculating the values of diffusion coefficient, D and N_0, corresponding to the number of the growth centers per unit area [58]:

$$D=\frac{J_{\max}^2 t_{\max}}{0.1629(zFC)^2} \tag{11}$$

and

$$N_0=0.065k^{-1/2}\left(\frac{zFC}{t_{\max}J_{\max}}\right)^2 \tag{12}$$

where $k=(8\pi CM/\rho)^{1/2}$, ρ is the cobalt molar density (151.03 mol/dm^3), and M is the relative molar mass of cobalt (58.93 g/mol).

Diffusion coefficients for the cobalt species were found from position of maximum of cathodic current on the chronoamperometric curves. The obtained results of 1.8×10^{-5} cm^2/s for pH 3 and 6.6×10^{-6} cm^2/s for pH 4 were in very good agreement with the data calculated upon Cottrell equation, while for other pH the values were $(4.2\pm1.8)\times10^{-6}$ cm^2/s. The latter can be explained again by hindering changes in the mass transport of the cobalt species resulting in the formation of the nucleation maxima on the J−t curves at longer time for higher pH.

The number density of the active centers (N_0) was calculated from the maximum peak coordinates on the J−t curves of initial stages of cobalt deposition. The obtained values of N_0 decreased from 3.6×10^5 cm^{-2} for pH 3 to 2.3×10^3 cm^{-2} for pH 7 confirming again inhibiting effect of cobalt gluconate complexes on the metal deposition. The

obtained results are quite comparable to those reported for the cobalt deposition from sulfate containing electrolytes (10^4−10^7 cm^{-2}) [56,59].

It should be emphasized that there is no one mechanism of the cobalt nucleation. The 3D instantaneous [17,56] or progressive [9,20,52] models were reported for electrolytes of various composition, at different deposition potentials and different substrates [59,60] or even investigation method [16,61]. Interestingly in the previous work [20] the progressive nucleation with diffusion limited growth was observed in the gluconate electrolytes (chloride, sulfate, chloride−sulfate) of pH 3.5. This different nucleation type evidently originated from the bath additives like ammonium salts, while they were absent in the current study. The current study partially confirmed the nucleation model in the sulfate−gluconate solution proposed earlier by EL REHIM et al [19], who identified instantaneous process under charge transfer control.

3.5 Cobalt electrodeposition

The potentiostatic electrodeposition of cobalt layers was performed. Figure 12(a) shows changes in the total and partial electric charge flowed through the system during electrolysis at constant time. It was observed that the current generated is dependent on the conductivity of the solution, and thus the lowest total charges were registered at pH (7±1), where movement of the main ionic charge carriers seemed to be the lowest. This slightly affected thickness of the metal deposits (4.6±1.2) μm; Fig. 12(a), but influenced cathodic current efficiency (25%−79%; Fig. 12(b)). Data shown in Fig. 12 indicate, in general, few ranges of deposition conditions originated from the bath specification, which then affect both morphology and crystal structure of the layers.

The cobalt deposits were matte gray and compact with no cracks or microcracks. Although the cathodic current efficiency was relatively low, no pitting was observed on the coating surface. This indicates fairly fast detachment of hydrogen bubbles from the cathode surface, especially as the electrolysis time was short enough to prevent metal build-up around the gas bubbles. Figure 13(a) shows surface morphologies of the coatings, which are evidently pH-dependent. Under the most acidic conditions the deposit shows ridge structure composed of a mixture of dense network of thin slabs incorporated into fine polyhedral grains. Interestingly, such ridge structure is typically observed for cobalt coatings produced from acidic chloride-containing electrolytes [5,6,62−64]. The elongated plate grains gradually disappeared and became less and less distributed on the coating surface as pH increased and were not observed for the highest pH values. Simultaneously, the deposits were composed of polyhedral fine grains of quite uniform dimensions. The size of the crystals increased for the most alkaline conditions and fairly large pyramidal grains were formed. The changes in the grain dimensions are reflected by roughness profiles (Table 3) performed by image analysis of the gray scale SEM micrograph areas. They give also estimated number of grains per unit area showing decreased amount of grains due to their larger dimensions. In all individual cases, the grains are packed densely and their sizes seem to be homogenous, and there is no visible large deviation in the dimensions. This is in a good agreement with the instantaneous nucleation of cobalt, where all nuclei form at the same time and then grow simultaneously. The pH ranges where the specific

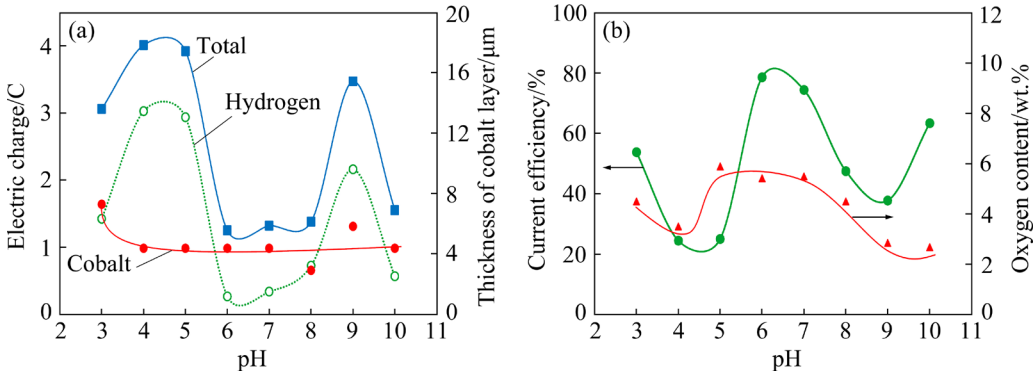

Fig. 12 Effect of pH on total and partial electric charges flowed during electrolysis and thickness of cobalt deposits (a) and cathodic current efficiency and oxygen contamination (b)

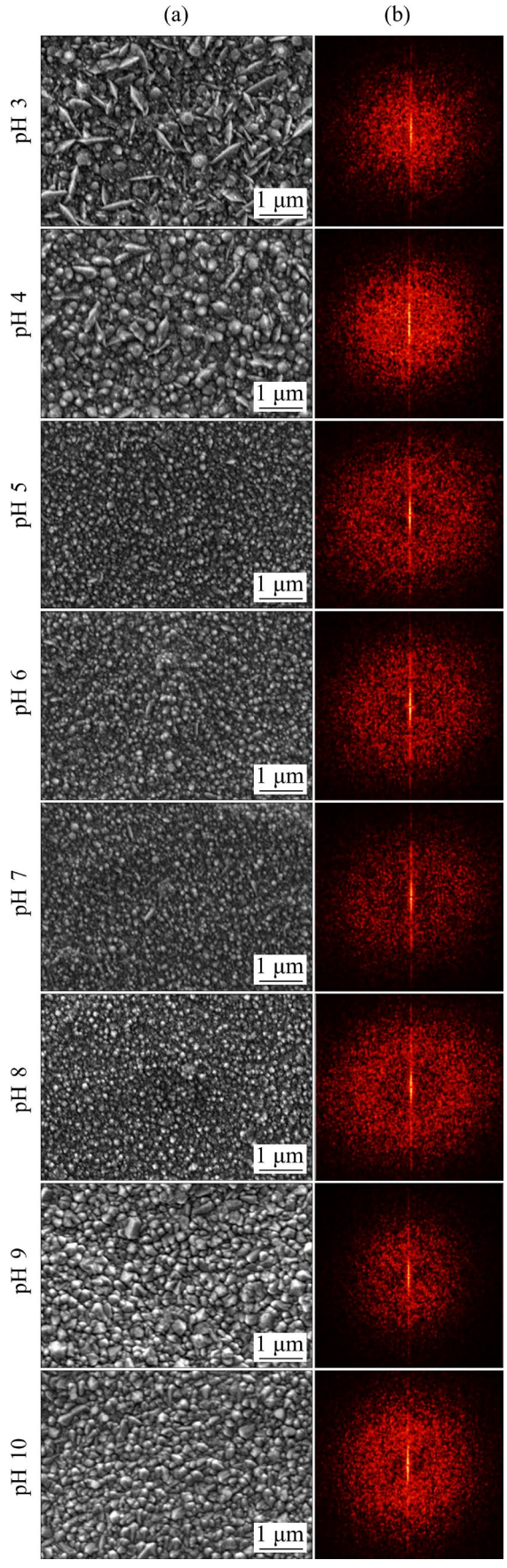

Fig. 13 SEM micrographs of cobalt surface (a) and their FFT analysis result (b)

Table 3 Roughness profiles of cobalt surfaces (image analysis)

pH	Roughness profile	R_a	N/μm^{-2}
3	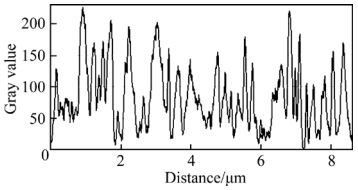	74.7	71
4	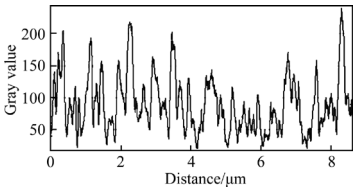	80.8	93
5	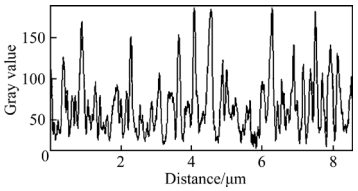	63.1	67
6	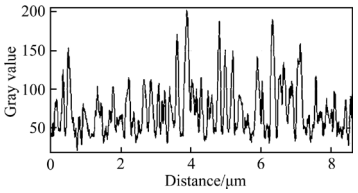	72.9	74
7	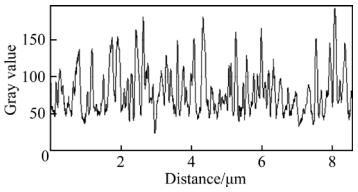	76.6	80
8	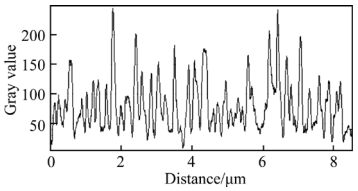	81.1	51
9	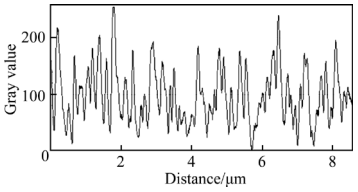	100.4	41
10	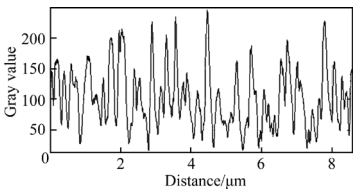	93.3	37

R_a—Arithmetic average of profile height deviation from mean line; N—Average grain number

changes in the coatings morphology were observed are also correlated with the changes in the nucleation and deposition potentials observed on CV curves (Fig. 7(d) inset) and the kinetic aspects of the deposition indicating effect of the course of the electrochemical reaction steps at the electrode surface on the development of the metal grains in the electrolyte containing various metal complexes. It can be emphasized that "ridge" morphology seen mainly under acidic conditions correlates with higher hydrogen evolution allowing cobalt to grow without any macroscopic blocks by the gas bubbles sticking on the electrode [8]. However, as pH increases to 5−8, the grain sizes decrease indicating inhibiting influence of adsorbed species, probably $CoOH^+$, and especially somewhat higher oxygen contents on the cobalt surface were detected (Fig. 12(b)). At the highest pH values, where the chemical reaction as a rate-determining step is postulated, the metal grains grow large of pyramid-like shape.

Figure 13(b) shows FFT patterns corresponding to the SEM images. The Fourier transform analyzes regularity of the grain arrangement and gives helpful information about the periodicity of a structure. FFT pattern modified as surface morphology changed with pH. Diffuse disk-shaped or ring-shaped forms in the FFT images represent non-ideal structure and suggest the presence of surface defects, irregularities in the structure and no directionality. However, in some cases slightly elongated ellipses can indicate some anisotropy, e.g. the grains can exhibit preferred orientation.

The modification of the surface morphology is further reflected by gradual changes of the cobalt crystal orientation. Figure 14 shows X-ray diffraction patterns, while Table 4 summarizes peak relative intensities. The results indicate formation of cobalt having hexagonal close packed (HCP) crystal lattice (Fig. 15(a)) with preferred plane orientations (Fig. 15(b)) dependent on the electrolyte pH (Table 4). For acidic pH, predominant orientation of the (0002) plane with the closest packing was observed, while relative intensities of the peaks for $(10\bar{1}0)$ and $(11\bar{2}0)$ planes gradually increased as pH increased up to 5. In turn, only one strong signal originating from the (0002) plane was observed for the deposit produced at pH 6. For pH 8 and higher the preferential orientation changed to the $(11\bar{2}0)$ plane.

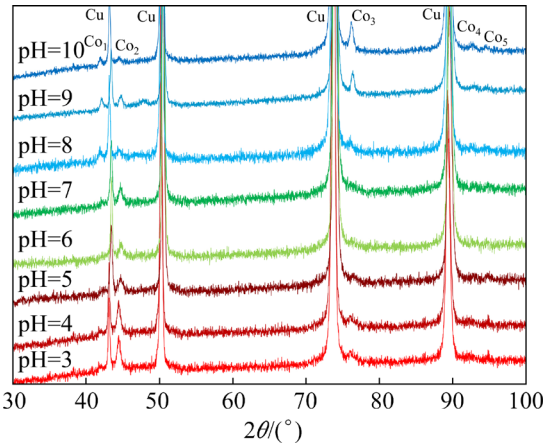

Fig. 14 X-ray diffraction patterns for cobalt deposits produced at various electrolyte pH (The assignment of (*hkil*) planes to Co_n characters can be found in Table 4)

Table 4 Analysis of XRD data and surface energy of HCP cobalt crystal facets

pH	Relative intensity, (I/I_{max})/%				
	Co_1 $(10\bar{1}0)$	Co_2 (0002)	Co_3 $(11\bar{2}0)$	Co_4 $(11\bar{2}2)$	Co_5 $(20\bar{2}1)$
3	15	100	14	–	–
4	23	23	23	23	23
5	40	100	38	–	–
6	–	100	–	–	–
7	10	100	19	–	–
8	91	73	100	36	36
9	66	59	100	26	26
10	33	24	100	29	19
Surface energy/ $(J\cdot m^{-2})$ [65]	2.26	2.10	2.45	2.58	2.39

The preferential growth of the (*hkil*) planes can be further completed quantitatively by the texture coefficients, $T_C(hkil)$ [66]:

$$T_C(hkil)=\frac{I(hkil)/I_0(hkil)}{\frac{1}{n}\sum[I(hkil)/I_0(hkil)]} \quad (13)$$

where n is the number of the diffraction peaks measured; $I(hkil)$ and $I_0(hkil)$ are intensities of the particular (*hkil*) reflections of the analyzed sample and the reference standard used (JCPDS card: 01-089-7094), respectively. If the values of $T_C(hkil)$ are closed to 1 for all the crystal planes considered, a randomly oriented crystallite structure similar to the reference standard is present in the investigated

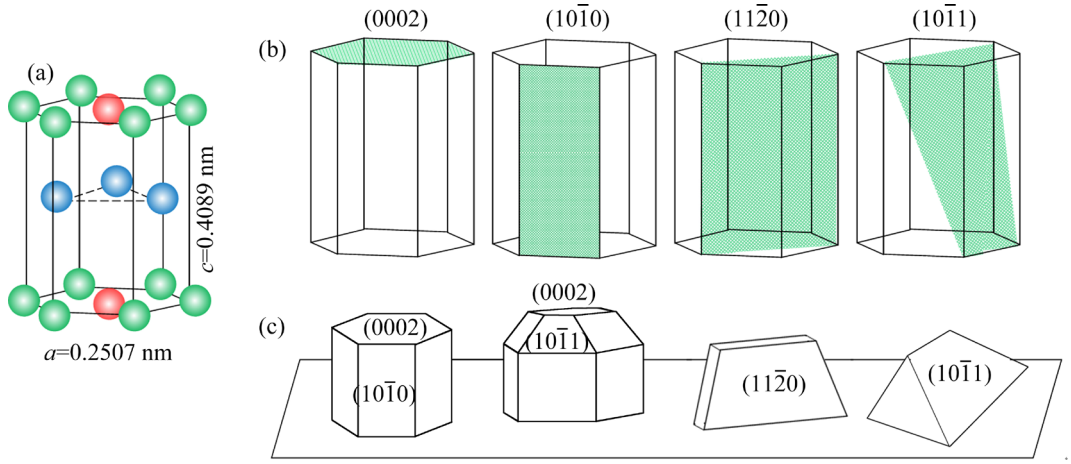

Fig. 15 HCP cobalt lattice (a), orientation of crystal planes (b), and possible crystal shapes (c)

sample. The $T_C(hkil)$ values ranging from 0 to 1 indicate the absence of grains oriented in that direction. On the other hand, the $T_C(hkil)$ values higher than 1 indicate an abundance of grains in a specific direction, and the higher the texture coefficient, more pronounced the preferential growth of crystallites in the direction perpendicular to the considered (*hkil*) plane. Table 5 gives the texture coefficients for the cobalt electrodeposits obtained in this study (possible maximal $T_C(hkil)$ value is 5.0, since five diffraction peaks were considered). The analysis of the data confirms pH-dependent preferential development of the (0002) and (11$\bar{2}$0) planes, with the latter being particularly noticeable for the most alkaline solutions, as indicated by the $T_C(hkil)$ values higher than 2.

Development of various preferential planes in the crystal lattice affects the growth of the metal crystals of various shapes (Fig. 15(c)) observed during formation of the cobalt deposits [16,62,63]. This is usually attributed to the adsorption of different species (e.g. H_{ads}, $CoOH^+_{ads}$, $Co(OH)_{2ads}$), which selectively induce slower growth of some planes and thus promote the formation of others [8,12,63]. It is known that the preferred crystallographic orientation follows tendency of minimization of surface energy during the electrodeposition process and the surface free energy mainly governs the crystal shape near equilibrium conditions. Mass transport and/or surface properties play a dominant role in forming the shape of deposited crystals when the process is realized at higher overpotential [67]. Table 4 shows values of surface energy for HCP cobalt crystal facets [65]. The development the crystal facets, originated from the existence of preferred (0002) plane orientation, have the lowest surface energy (2.10 J/m^2) and is predominate under the acidic conditions, where the electroreduction of Co^{2+} from relatively labile complexes is not seriously affected by the stage of the cation release from the complex. Gradual change in the bath pH influences the bath speciation (Figs. 2 and 6) and the path of the nucleation and growth (Fig. 9) resulting in the modification of preferred orientation into the (11$\bar{2}$0) plane. The corresponding crystal facet showing higher surface energy (2.45 J/m^2) may exhibit greater activity in adsorption processes, which affect their ability to accept ions from the solution, and especially the chemical reaction (reaction overpotential) as a rate-determining step was established. This is consistent with the discussion of the Tafel slopes presented above. However, it must be stated that surface free

Table 5 Texture coefficients calculated upon XRD data (Table 4) and JCPDS standard (01-089-7094)

pH	$T_C(hkil)$				
	Co_1 (10$\bar{1}$0)	Co_2 (0002)	Co_3 (11$\bar{2}$0)	Co_4 (11$\bar{2}$2)	Co_5 (20$\bar{2}$1)
3	0.2	5.0	1.8	0.0	0.0
4	0.6	2.6	1.7	0.0	0.0
5	0.8	2.2	2.0	0.0	0.0
6	0.0	5.0	0.0	0.0	0.0
7	0.5	2.9	1.6	0.0	0.0
8	0.7	0.5	2.1	0.8	0.8
9	0.6	0.5	2.5	0.7	0.7
10	0.4	0.2	2.9	0.9	0.6

energies are not same in vacuum and electrolytes, since adsorption of ions in electrolytes reduces the surface free energy. It is commonly explained that surface energy increases for orientations with more open planes (least dense planes) [68]. The results obtained in this study can be compared with the data reported by NAKANO et al [64]. They found that the crystal orientation of HCP cobalt deposits produced from sulfate bath was overpotential-dependent and the (0002) plane was preferentially oriented in the low overpotential range, while the preferred orientation of the $(11\bar{2}0)$ plane became noticeable with increased overpotential. Analysis of the data suggests that observed transition from one to another favored growth and thus changes in the deposit morphology can originate from adsorption of different species, possibly $CoOH^+$ intermediate.

It can be noted that although stable form of cobalt is the HCP phase [2,20,21,64], a mixture of HCP and FCC (face centered cubic) or even pure FCC structure can be found in the cobalt deposits [19,62,63]. Interestingly, EL REHIM et al [19] identified a mixture of phases in the compact microcracked and fine grained cobalt produced from acidic sulfate−gluconate baths at constant currents. This differs from the current data, but is understandable, since structural and morphological differences between galvanostatic and potentiostatic depositions are observed [61].

3.6 Anodic stripping analysis

Figure 16 shows results of the anodic stripping for thin cobalt layers. They represent single peak at the potential of about −0.1 V corresponding to the dissolution of cobalt if produced at pH 3−7. The course of anodic curves changed for higher pH, where lower and wider peak develops with a maximum at the potential of −0.3 V. It is followed by secondary peaks at more positive potential values, but their height decreases with the electrolyte alkalization. The obtained results are correlated with the structures of the deposits dependent on the bath speciation. It seems that high anodic peaks develop due to dissolution of cobalt of preferential crystal orientations followed by more or less easy formation of the soluble intermediates.

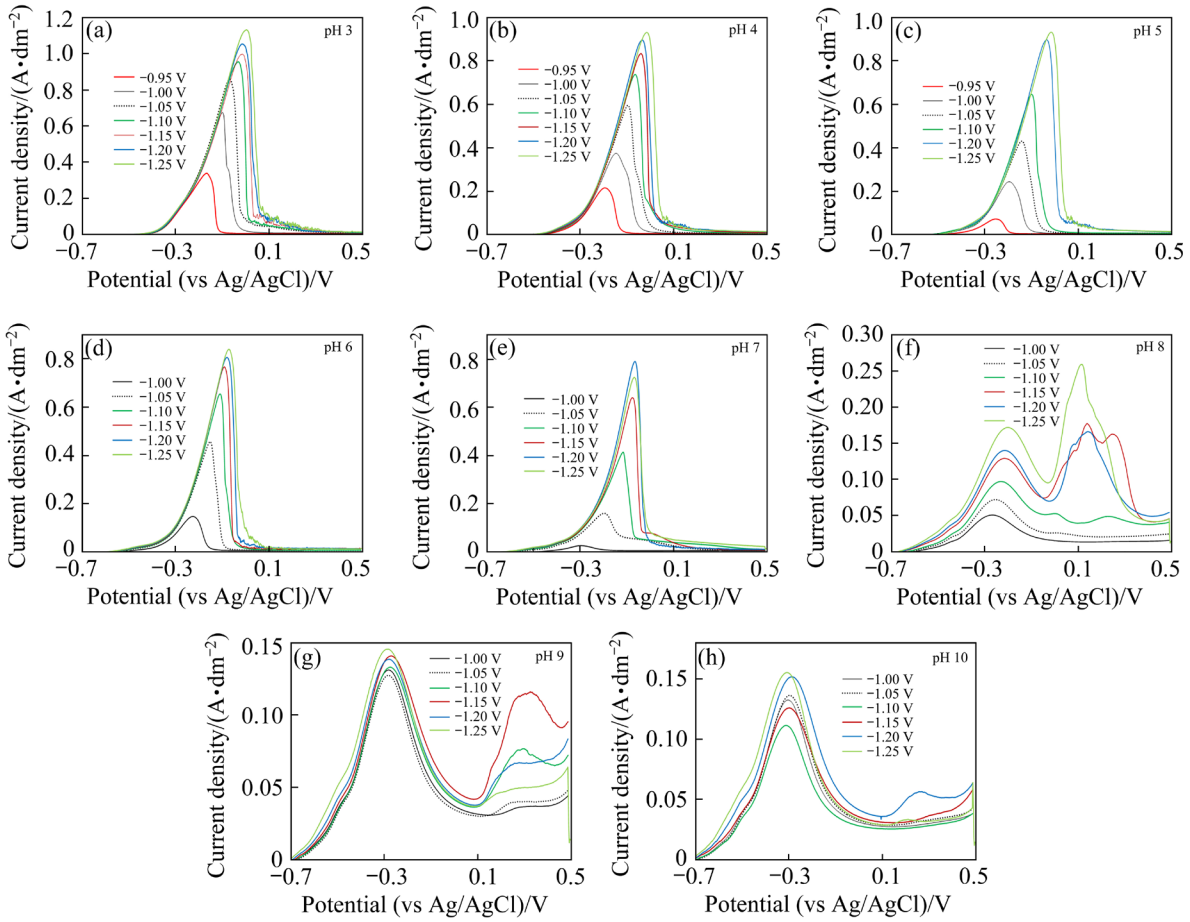

Fig. 16 Anodic sweep analysis results of cobalt thin layers: (a) pH 3; (b) pH 4; (c) pH 5; (d) pH 6; (e) pH 7; (f) pH 8; (g) pH 9; (h) pH 10

4 Conclusions

(1) The complexation of cobalt(II) ions by gluconate ions is dependent on the electrolyte pH giving a variety of species with different structures and various contents in the solution.

(2) Buffering properties of the electrolyte towards acid and base addition are affected by the pH due to multiple ionic equilibria involving cobaltous, gluconate and boric acid species.

(3) Cobalt−gluconate complexes affect rate-determining step of the electroreduction in various ways: the cathodic process run under activation control followed by diffusion control in acidic range, while it changes into reaction control at higher pH.

(4) Potentiostatic formation of the cobalt deposits run via 3D instantaneous nucleation followed by diffusion controlled growth, but it is disturbed at higher pH due to a release of the metal cation from gluconate complexes as a limiting step.

(5) pH-dependent morphology and crystal planes of preferred orientation of HCP cobalt deposits were correlated with the bath speciation and kinetic aspects of the cathodic reaction. However, at this moment it is not definitely clear what type of adsorbate species ($CoOH^+$ is believed at pH 5−8) governs the structural changes.

CRediT authorship contribution statement

Ewa RUDNIK: Conceptualization, Methodology, Resources, Investigation, Data curation, Calculations, Data analysis, Validation, Visualization, Writing − Original draft preparation, Writing − Reviewing and editing.

Declaration of competing interest

The author declares that he has no known competing financial interests or personal relationships that could have appeared to influence the work reported in this paper.

Acknowledgments

Author wishes to thank Monika HAŁACIŃSKA and Grzegorz WŁOCH for their technical help.

References

[1] GARCIÁ-TORRES L, GÓMEZ E, VALLÉS E. Modulation of magnetic and structural properties of cobalt thin films by means of electrodeposition [J]. Journal of Applied Electrochemistry, 2009, 39: 233−240.

[2] SZMAJA W, KOZŁOWSKI W, POLAŃSKI K, BALCERSKI J, CICHOMSKI M, GROBELNY J, ZIELIŃSKI M, MIĘKOŚ E. Investigation of thick cobalt films electrodeposited on gold substrates [J]. Chemical Physics Letters, 2012, 542: 117−122.

[3] CAFFARENA V R, GUIMARÃES A P, FOLLY W S D, SILVA E M, CAPITANEO J L. Magnetic behavior of electrodeposited cobalt nanowires using different electrolytic bath acidities [J]. Materials Chemistry and Physics, 2008, 107: 297−304.

[4] EZHILSELVI V, SEENIVASAN H, BERA P, ANANDAN C. Characterization and corrosion behavior of Co and Co−P coatings electrodeposited from chloride bath [J]. RSC Advances, 2014, 4: 46293−46304.

[5] BURZYŃSKA L, RUDNIK E, BŁAŻ L, SZYMAŃSKI W, JĘDRAS S. Influence of electrolysis parameters on the content of dispersion particles in Co−SiC composites [J]. Archives of Metallurgy and Materials, 2009 54(1): 47−56.

[6] RUDNIK E, BURZYŃSKA L, JĘDRUCH J, BŁAŻ L. Codeposition of SiC particles with electrolytic cobalt in the presence of Cs^+ ions [J]. Applied Surface Science, 2009, 255(16): 7164−7171.

[7] PATNAIK P, TRIPATHY B C, BHATTACHARYA I N, PARAMGURU R K, MISHRA B K. Effect of tetra propyl ammonium bromide during cobalt electrodeposition from acidic sulfate solutions [J]. Metallurgical and Materials Transactions B, 2015, 46B: 1252−1256.

[8] MATSUSHIMA H, ISPAS A, BUND A, PLIETH W, FUKUNAKA Y. Magnetic field effects on microstructural variation of electrodeposited cobalt films [J]. Journal of Solid State Electrochemistry, 2007, 11: 737−747.

[9] CUI C Q, JIANG S P, TSEUNG A CC. Electrodeposition of cobalt from aqueous chloride solutions [J]. Journal of the Electrochemical Society, 1990, 137(11): 3418−3423.

[10] KONGSTEIN O E, HAAREBERG G M, THONSTAD J. Current efficiency and kinetics of cobalt electrodeposition in acid chloride solutions. Part I: The influence of current density, pH and temperature [J]. Journal of Applied Electrochemistry, 2007, 37: 669−674.

[11] MATSUSHIMA J T, TRIVINHO-STRIXINO F, PEREIRA E C. Investigation of cobalt deposition using the electrochemical quartz microbalance [J]. Electrochimica Acta, 2006, 51: 1960−1966.

[12] FLIS-KABULSKA I. Electrodeposition of cobalt on gold during voltammetric cycling [J]. Journal of Applied Electrochemistry, 2006, 36: 131−137.

[13] SANTOS J S., MATOS R, TRIVINHO-STRIXINO F, PEREIRA E C. Effect of temperature on Co electrodeposition in the presence of boric acid [J]. Electrochimica Acta, 2007, 53: 644−649.

[14] KONGSTEIN O E, HAAREBERG G M, THONSTAD J. Current efficiency and kinetics of cobalt electrodeposition in acid chloride solutions. Part II: The influence of chloride and

sulphate concentrations [J]. Journal of Applied Electrochemistry, 2007, 37: 675−680.

[15] MENDOZA-HUIZAR L H, RIOS-REYES C H. Cobalt electrodeposition onto polycrystalline gold from ammoniacal solutions [J]. Central European Journal of Chemistry, 2013, 11(8): 1381−1382.

[16] GRUJICIC D, PESIC B. Electrochemical and AFM study of cobalt nucleation mechanisms on glassy carbon from ammonium sulfate solutions [J]. Electrochimica Acta, 2004, 49: 4719−4732.

[17] FRANK A C, SUMODJO P T A. Electrodeposition of cobalt from citrate containing baths [J]. Electrochimica Acta, 2014, 132: 75−82.

[18] EL REHIM S S A, EL WAHAAB S M A, IBRAHIM M A M, DANKERIA M M. Electroplating of cobalt from aqueous citrate baths [J]. Journal of Chemical Technology and Biotechnology, 1998, 73(4): 369−376.

[19] EL REHIM S S A, IBRAHIM M A M, DANKERIA M M. Electrodeposition of cobalt from gluconate electrolyte [J]. Journal of Applied Electrochemistry, 2002, 32: 1019−1027.

[20] RUDNIK E, DASHBOLD N. Effect of Cl^- and SO_4^{2-} ions on electrodeposition of cobalt from acidic gluconate solutions [J]. Russian Journal of Electrochemistry, 2019, 55(12): 1305−1319.

[21] IBRAHIM M A M, AL RADADI R M. Nanocrystalline cobalt coatings on copper substrates by electrodeposition from complexing acidic glycine baths [J]. Materials Chemistry and Physics, 2015, 151: 222−232.

[22] CRITELLI R A J, SUMODJO P T A. Influence of glycine as additive in cobalt electrodeposition [J]. ECS Transactions, 2013, 50(52): 75−82.

[23] CANETE-RODRÍGUEZ A M, SANTOS-DUENAS I M, JIMÉNEZ-HORNERO J E, EHRENREICH A, LIEBL W, GARCÍA-GARCÍA I. Gluconic acid: Properties, production methods and applications—An excellent opportunity for agro-industrial by-products and waste bio-valorization [J]. Process Biochemistry, 2016, 51: 1891−1903.

[24] SAWYER D T. Metal-gluconate complexes [J]. Chemical Reviews, 1964, 64: 633−643.

[25] RUDNIK E. Effect of anions on the electrodeposition of tin from acidic gluconate baths [J]. Ionics, 2013, 19(7): 1047−1059.

[26] RUDNIK E. Effect of gluconate ions on electroreduction phenomena during manganese deposition on glassy carbon in acidic chloride and sulfate solutions [J]. Journal Electroanalytical Chemistry, 2015, 741: 20−31.

[27] RUDNIK E, CHAT K, WŁOCH G, OSUCH P. Influence of chloride and sulphate ions on electrodeposition, wettability and corrosion resistance of zinc coatings produced from gluconate solutions [J]. Journal of the Electrochemical Society, 2019, 166(8): D323−D332.

[28] RUDNIK E, WŁOCH G. The influence of sodium gluconate on nickel and manganese codeposition from acidic chloride-sulfate baths [J]. Ionics, 2014, 20(12): 1747−1755.

[29] GOMEZ E, GUAUS E, TORRENT J, ALCOBE X, VALLES E. Tin−cobalt electrodeposition from sulfate−gluconate baths [J]. Journal of Applied Electrochemistry, 2001, 31: 349−354.

[30] SEENIVASAN H, BERA P, RAJAM K S, PARIDA S K. Characterization and hardness of Co−P coatings obtained from direct current electrodeposition using gluconate bath [J]. Surface Review and Letters, 2013, 20(5): 1350049: 1−12.

[31] EBRAHIMIFAR H, ZANDRAHIMI M. Influence of electrodeposition parameters on the characteristics of Mn−Co coatings on Crofer 22 APU ferritic stainless steel [J]. Bulletin of Material Science, 2017, 40(6): 1273−1283.

[32] WESTON D P, HARRIS S J, SHIPWAY P H, WESTON N J, YAP G N. Establishing relationships between bath chemistry, electrodeposition and microstructure of Co−W alloy coatings produced from a gluconate bath [J]. Electrochimica Acta, 2010, 55: 5695−5708.

[33] SHUL'MAN A I, BELEVSKII S S, YUSHCHENKO S P, DIKUSAR A I. Role of complexation in forming composition of Co−W coatings electrodeposited from gluconate electrolyte [J]. Surface Engineering and Applied Electrochemistry, 2014, 50(1): 9−17.

[34] BOBANOVA Z I, PETRENKO V I, VOLODINA G F, KROITORU D M, DIKUSAR A I. The effect of the pH on the composition and properties of Co−W alloys manufactured from gluconate electrolyte [J]. Surface Engineering and Applied Electrochemistry, 2015, 51(1): 25−37.

[35] The UPAC stability constants database. Academic Software and IUMAC, 1992—2000 [R].

[36] KUTUS B, GAONA X, PALLAGI A, PÁLINKÓ I, ALTMAIER M, SIPOS P. Recent advances in the aqueous chemistry of the calcium(II)−gluconate system–Equilibria, structure and composition of the complexes forming in neutral and in alkaline solutions [J]. Coordination Chemistry Reviews, 2020, 417: 213337.

[37] ASHTON F, PICKERING W F. Cobalt(II) gluconate complexes [J]. Australian Journal of Chemistry, 1970, 23(7): 1367−1373.

[38] SAWYER D T, BAGGER J B. The lactone-acid-salt equilibria for D-Glucono-δ-lactone and the hydrolysis kinetics for this lactone [J]. Journal of the American Chemical Society, 1959, 81(20): 5302−5306.

[39] ESCANDAR G M., PEREGRIN J M S, GONZALEZ SIERRA M, MARTINO D, SANTORO M, FRUTOS A A, GARCIA S I, LABADIE G, SALA F L. Interaction of divalent metal ions with D-gluconic acid in the solid phase and aqueous solution [J]. Polyhedron, 1996, 15(13): 2251−2261.

[40] WARWICK P, EVANS N, VINES S. Studies on metal gluconic acid complexes [C]//van ISHEGHEM P. Scientific Basis for Nuclear Waste Management XXIX, Materials Resource Society Symposium Proceedings, 932, Warrendale, PA, 2006: 959−966.

[41] PERKAMPUS H H. UV-Vis spectroscopy and its applications [M]. Berlin-Heildelberg: Springer Verlag, 1992.

[42] PETKOVA P, NEDKOV V. Behavior of Co^{2+} cations in the aqueous and alcoholic solution of $CoCl_2·6H_2O$ [J]. Acta

Physica Polonica A, 2013, 123(2): 207−208.

[43] CRITELLI R A J, SUMODJO P T A. Influence of glycine as additive in cobalt electrodeposition: IR spectroscopy and near-surface pH investigations [J]. Electrochimica Acta, 2018, 260: 762−771.

[44] JIANG S P, TSEUNG A C C. Reactive deposition of cobalt electrode III. Role of anions [J]. Journal of the Electrochemical Society, 1990, 137(11): 3387−3393.

[45] FRANCZAK A, BOHR F, LEVESQUE A, CHOPART J P. Quantum chemical study of hydrogen evolution during cobalt electrodeposition [J]. Research & Reviews: Journal of Chemistry, 2015, 4(4): 74−86.

[46] ALLONGUE P, CAGNON L, GOMES C, GÜNDEL A, COSTA V. Electrodeposition of Co and Ni/Au(111) ultrathin layers. Part I: Nucleation and growth mechanism from in situ STM [J]. Surface Science, 2004, 557: 41−56.

[47] KOCHKODAN V, DARWISH N B, HILAL N. The chemistry of boron in water [M]//KABAY N, BRYJAK M, HILAL N. Boron Separation Processes, Amsterdam: Elsevier, 2015: 35−63.

[48] SASIDHARANPILLAI S, ARCIS H, TREVANI L, TREMAINE P R. Triborate formation constants and polyborate speciation under hydrothermal conditions by Raman spectroscopy using a titanium/sapphire flow cell [J]. The Journal of Physical Chemistry B, 2019, 123: 5147−5159.

[49] PALMER D A, BENEZETH P, WESOŁOWSKI D J. Boric acid hydrolysis: A new look at the available data [J]. Powerplant Chemistry, 2000, 2: 261−264.

[50] RUDNIK E, WOJNICKI M, WŁOCH G. Effect of gluconate addition on the electrodeposition of nickel from acidic baths [J]. Surface and Coatings Technology, 2012, 207: 375−388.

[51] NOEL M, VASU K I. Cyclic voltammetry and the frontiers of electrochemistry [M]. Edinburgh: Aspect Publications, 1990.

[52] SOTO A B, ARCE E M, PALOMAR-PARDAVÉ M, GONZALEZ I. Electrochemical nucleation of cobalt on glassy carbon electrode from ammonium chloride solutions [J]. Electrochimica Acta, 1996, 41(6): 2647−2655.

[53] CASELLA I G, CONTURSI M. Cobalt oxide electrodeposition on various electrode substrates from alkaline medium containing Co–gluconate complexes: A comparative voltammetric study [J]. Journal of Solid State Electrochemistry, 2012, 66: 3739−3764.

[54] GUIDELLI R, COMPTON R G, FELIU J M, GILEADI E, LIPKOWSKI J, SCHMICKLER W, TRASATTI S. Defining the transfer coefficient in electrochemistry: An assessment (IUPAC Technical Report) [J]. Pure Applied Chemistry, 2014, 86(2): 245−258.

[55] LEFEBVRE M C. Establishing the link between multistep electrochemical reaction mechanisms and experimental Tafel slopes [M]//CONWAY B E, BOCKRIS J O'M, WHITE R E. Modern Aspects of Electrochemistry. Vol. 32. New York: Kluwer Academic/Plenum, 2002: 249−300.

[56] MENTAR L, KHELLADI M R, AZIZI A, KAHOUL A. Effect of potential on the early stages of nucleation and growth during cobalt electrocrystallization in sulfate medium onto FTO surface [J]. Materials Letters, 2010, 64: 2403−2406.

[57] SURVILA A, STASIKAITIS P V. Linear potential sweep voltammetry of electroreduction of labile complexes—I. Background model [J]. Electrochimica Acta, 1997, 42(7): 1113−1119.

[58] SHARIFKER B R, HILLS G. Theoretical and experimental studies of multiple nucleation [J]. Electrochimica Acta, 1983, 28(7): 879−889.

[59] RIOS-REYES C H, MENDOZA-HUISAR L H, RIVERA M. Electrochemical kinetic study about cobalt electrodeposition onto GCE and HOPG substrate from sulfate sodium solutions [J]. Journal of Solid State Electrochemistry, 2010, 14: 659−668.

[60] SAHARI A, AZIZI A, FENINECHE N, SCHMERBER G, DINIA A. Electrochemical study of cobalt nucleation mechanisms on different metallic substrates [J]. Materials Chemistry and Physics, 2008, 108: 345−352.

[61] MANHABOSCO T M, ENGLERT G, MÜLLER I L. Characterization of cobalt thin films electrodeposited onto silicon with two different resistivities [J]. Surface and Coatings Technology, 2006, 200: 5203−5209.

[62] GOMEZ E, VALLES E. Thick cobalt coatings obtained by electrodeposition [J]. Journal of Applied Electrochemistry, 2002, 32: 693−700.

[63] VINCENZO A, CAVALLOTTI P L. Growth modes of electrodeposited cobalt [J]. Electrochimica Acta, 2004, 49: 4079−4089.

[64] NAKANO H, NAKAHARA K, KAWANO S, OUE S, AKIYAMA T, FUKUSHIMA H. Effect of electrolysis factors on crystal orientation and morphology of electrodeposited cobalt [J]. Journal of Applied Electrochemistry, 2002, 32: 43−48.

[65] LIN Hao, LIU Jin-xun, FAN Hong-jun, LI Wei-xue, Compensation between surface energy and hcp/fcc phase energy of late transition metals from first-principles calculations [J]. Journal of Physical Chemistry C, 2020, 124: 11005−11014.

[66] GARRET C S, MASSALSKI T B. Structure of metals [M]. Oxford: Pergamon Press, 1980.

[67] GUO L, OSKAM G, RADISIC A, HOFFMANN P M, SEARSON P C. Island growth in electrodeposition [J]. Journal of Physics D: Applied Physics, 2011, 44: 443001.

[68] KRAUSE A, UHLEMANN M, GEBERT A, SCHULTZ L. A study of nucleation, growth, texture and phase formation of electrodeposited cobalt layers and the influence of magnetic fields [J]. Thin Solid Films, 2006, 515: 1694−1700.

pH 依赖型镀液成分对从硫酸盐−葡萄糖酸盐溶液中电沉积钴的影响

Ewa RUDNIK

Faculty of Non–Ferrous Metals, AGH University of Krakow, Al. Mickiewicza 30, 30-059 Krakow, Poland

摘　要：采用文献中的稳定常数，计算硫酸钴−葡萄糖酸盐溶液中 pH 依赖的多重平衡。通过分光光度实验和溶液缓冲特性分析(pH 3−10)，讨论了镀液成分及含量随 pH 的变化。循环伏安法测试结果表明，由于电解质中不同的离子组成，含钴物质的电化学行为发生了变化。计算了塔菲尔斜率，并讨论了含钴物质的电还原过程。计时安培研究显示，钴沉积的机制为三维瞬时形核和受扩散控制的长大过程，但在较高 pH 条件下阳离子从葡萄糖酸配合物中释放出来导致该过程受阻。测定了含钴物质的扩散系数。pH 值的变化还反映在镀层形貌(SEM)的变化、择优取向面的发展(XRD、织构系数)以及电流效率上，但在−1.0 V(vs Ag/AgCl)恒定电位下沉积的镀层厚度并未发生显著变化。阳极析出分析表明，钴镀层中择优取向面的存在导致了阳极响应的变化。

关键词：钴；电沉积；形核；成分；结构

(Edited by Bing YANG)